JMEPEG (2011) 20:177–184
DOI: 10.1007/s11665-010-9672-7

1059-9495/$19.00

Texture Prediction of Cold- and Hot-Rolled Titanium Using Processing Path Model

J. Bouhattate, D.S. Li, Gilberto A. Castello Branco, Cristiane M.B. Bacaltchuk, and H. Garmestani

(Submitted September 17, 2009; in revised form April 1, 2010)

Titanium alloys have very attractive properties, which are highly dependent on the material microstructure. Accurately predicting the microstructure of such materials during processing for materials design is, therefore, very important. In this study, texture evolution of titanium alloys cold rolled at room temperature and hot rolled at 260 °C is simulated using a processing path model. Texture coefficients, a set of weights in spherical harmonics expansion of texture, are utilized as descriptors of materials to represent the texture state of polycrystalline materials during processing. This model is based on the conservation principle in the orientation space. Deriving from experimental texture input at different deformation stages, the texture evolution matrix was calculated. This matrix is used to predict texture evolution for the specified deformation mode. The simulated texture evolution results agree well with experimental results.

Keywords materials design, processing path model, spherical harmonics, texture, titanium

1. Introduction

Titanium and titanium alloys are used in a wide variety of aerospace, energy, and biomedical applications. They have very attractive properties, such as high specific strength, elastic modulus, and fracture toughness (Ref 1). These properties are highly dependent on the material's microstructure, i.e., texture, dislocation density, and dislocation slip system activity. Therefore, in order to be able to predict performance of the materials and also to design materials with specific properties, a fundamental understanding of the deformation process in terms of microstructural parameters is critical.

Microstructure sensitive design (MSD) for polycrystalline materials has remarkably evolved during the past years (Ref 2-10). This model provides a rigorous mathematical framework for design and development of new materials by finding the possible microstructures that yield desired performance for the target application. Microstructure is represented by a Fourier expansion: the weights of the expansion are used to represent the microstructure, while all the possible microstructure are enclosed in a "materials hull" in this Fourier space. This exploits the fact that all aspects of materials design can be carried out efficiently in a common Fourier space.

Different processing options used to realize the preferred microstructures are also explored in this Fourier space. The evolution of texture during mechanical deformation can be represented as a path line (processing path) in the microstructure hull. Each point in this Fourier space stands for a unique texture associated with corresponding properties. For materials system with cubic crystal symmetry and orthotropic sample symmetry, the relevant part of the Fourier space reduces to three dimensions; for materials system with hcp crystal symmetry and orthotropic sample symmetry, it reduces to five dimensions. The method used to determine the boundaries of the microstructure hull is derived from the Gram-Schmidt orthonormalization theory. The detailed study was presented by Lyon and Adams (Ref 9) for fcc crystal symmetry systems, and by Proust and Kalidindi (Ref 10) for hcp crystal symmetry materials.

Modeling texture evolution is an important issue in MSD. In titanium alloys, it has been approached by many different methods. A few examples include Taylor-type model (Ref 11), phase field model (Ref 12), Monte Carlo method (Ref 13), self-consistent model (Ref 14), and hybrid model (Ref 15). In this study, texture evolution is modeled by using processing path model, based on a conservation principle of texture proposed by Clement and Coulomb (Ref 16, 17). It has been applied in our previous studies (Ref 4-8) to simulate texture evolution during deformation in cubic and hexagonal materials. This model was also used to give an optimal processing path through a streamline family of processing paths. In the following, this model is examined further to simulate texture evolution of cold- and hot-rolled titanium using experimental data.

2. Processing Path Model

In processing path model, Fourier expansion had been used to approximate the texture and the associated properties of materials. The particular basis functions used in this study are

J. Bouhattate, Laboratoire d'études des Matériaux en milieux agressifs (LEMMA), Université de La Rochelle, Av. Michel Crépeau, 17042 La Rochelle, France; **D.S. Li**, Fundamental and Computational Sciences Directorate, Pacific Northwest National Laboratory, Richland, WA 99352; **Gilberto A. Castello Branco** and **Cristiane M.B. Bacaltchuk**, CEFET-RJ, Program of Mechanical Engineering and Materials Technology, Av. Maracanã 229, Bloco E sala E-312, Maracanã, Rio de Janeiro, RJ CEP 20271-110, Brazil; and **H. Garmestani**, School of Materials Science and Engineering, Georgia Institute of Technology, 771 Ferst Dr. N.W., Atlanta, GA 30332-0245. Contact e-mails: jamaa.bouhattate@univ-lr.fr, dongsheng.li@pnl.gov, hamid.garmestani@mse.gatech.edu.

known as the generalized spherical harmonic functions. There are several advantages in using these functions: (i) all the tensorial properties can be expressed using a finite number of terms; (ii) invertible relations between properties and textures may be derived; and (iii) all possible textures can be bounded in the Fourier space.

In processing path model, texture is represented by a set of spherical haromincs weight. These spherical harmonics weights compose of a space representing texture. If dV represents the totality of all volume elements in the sample that possesses the orientation g within the element of orientation dg, and V represents the total sample volume, then the texture orientation distribution function (ODF) $f(g)$ is represented by

$$f(g) = \frac{dV(g)}{Vdg} = f(\phi_1, \phi, \phi_2) = \sum_{l=0}^{\infty} \sum_{m=0}^{M(l)} \sum_{n=0}^{N(l)} F_l^{mn} \dot{\dot{T}}_l^{mn}(g) \quad \text{(Eq 1)}$$

where ϕ_1, ϕ, and ϕ_2 are Euler angles representing the orientation g.

Texture is commonly represented as a Fourier expansion of generalized spherical harmonics weighted by appropriate texture coefficients, F_l^{mn} (Ref 18-20). Texture coefficients are important in determining the properties of polycrystalline materials. The properties of polycrystalline materials can be represented as a summation of the product of property coefficients and spherical harmonics:

$$\bar{e} = \sum_{l=0}^{\infty} \sum_{m=o}^{M(l)} \sum_{n=0}^{N(l)} \bar{e}_l^{\mu\nu} \dot{\dot{T}}_l^{mn}(g) \quad \text{(Eq 2)}$$

While the property coefficients of a single crystal are constants, the property coefficients of a polycrystalline material, $\bar{e}_l^{\mu\nu}$, are dependent directly on the texture coefficients, $F_l^{\lambda\nu}$.

$$\bar{e}_l^{\mu\nu} = \frac{1}{2l+1} \sum_{\lambda=1}^{M(l)} \bar{e}_l^{\mu\lambda} F_l^{\lambda\nu}, \quad 0 \le l \le r \quad \text{(Eq 3)}$$

where r is the limit of order dependent on the crystal symmetry, sample symmetry and the property e.

The generalized spherical harmonics are the matrix elements of the irreducible representation of the 3D rotation group. They are defined by

$$\dot{\dot{T}}_l^{mn}(g) = \dot{\dot{T}}_l^{mn}(\phi_1, \phi, \phi_2) = e^{im\phi_1} P_l^{mn}(\cos\phi) e^{in\phi_1} \quad \text{(Eq 4)}$$

where P is the Legendre Polynomial:

$$P_l^{mn}(x) = \frac{(-1)^{l-m} i^{n-m}}{2^l (l-m)!} \left[\frac{(l-m)!(l+n)!}{(l+m)!(l-n)!}\right]^{1/2} (1-x)^{-\frac{n-m}{2}} \times (1+x)^{-\frac{n+m}{2}} \frac{d^{l-n}}{dx^{l-n}} \left[(1-x)^{l-m}(1+x)^{l+m}\right] \quad \text{(Eq 5)}$$

2.1 Microstructure Hull

Using the set of texture coefficients as a descriptor, microstructures can be represented as points in a multidimensional space composed by texture coefficients (Ref 2, 3). The number of dimensions depends on the number of texture coefficients used. Bunge (Ref 19) proved that an expansion of the Fourier series up to $\ell = 4$ is sufficient to explore elastic properties. For cubic materials, this means a total of four texture coefficients: F_0^{11}, F_4^{11}, F_4^{12}, and F_4^{13}; whereas for hcp materials, six will be needed: F_0^{11}, F_2^{11}, F_2^{12}, F_4^{11}, F_4^{12}, and F_4^{13}. Of these coefficients, the first one, F_0^{11}, is always equal to 1.

For cubic materials, the number of non-zero texture coefficients for an expansion of Fourier series, up to ℓ equal to 22, is 172; however, hcp materials have 351 texture coefficients. These texture coefficients have been used in this study to accurately predict texture evolution.

2.2 Evolution of Texture Coefficient During Plastic Deformation

Using the conservation principle in the orientation space, a set of relationships for the evolution of texture coefficients can be derived. A formulation is presented here for the streamlines as an analytical form among the texture coefficients for any specific thermo-mechanical process. In the formulation presented here, η is used as an appropriate metric of the process. For example, in the case of uniaxial tension, η represents the extension strain, and in the case of compression, η represents the compression ratio. The texture descriptor used in this study is a set of texture coefficients, $F_l^{mn}(\eta)$, that changes as a function of the processing parameter η. $f(g,\eta)$ is used to represent texture as a function of processing parameter η. As shown in the following equation, texture at any η can be expressed as a series of generalized spherical harmonic functions in which F_l^{mn} are the weights (coefficients) of $\dot{\dot{T}}_l^{mn}(g)$, the symmetric generalized spherical harmonics for the corresponding sample and crystal symmetry:

$$f(g,\eta) = \sum_{l=0}^{\infty} \sum_{m=0}^{M(l)} \sum_{n=0}^{N(l)} F_l^{mn}(\eta) \dot{\dot{T}}_l^{mn}(g) \quad \text{(Eq 6)}$$

For a single crystal orientation distribution in which all the crystals are oriented along g_i, texture coefficients F_l^{mn} are calculated directly from the spherical harmonics:

$$F_l^{mn} = (2l+1) \dot{\dot{T}}_l^{mn}(g_i) \quad \text{(Eq 7)}$$

Texture measured from x-ray diffraction or electron backscatter diffraction (EBSD) gives the volume fraction of the material with orientation g_i (Ref 21, 22). F_l^{mn} may be calculated from $f(g)$ and spherical harmonics as in Eq 8:

$$F_l^{mn} = (2l+1) \sum_i f(g_i) \dot{\dot{T}}_l^{mn}(g_i) \quad \text{(Eq 8)}$$

In Clement's study (Ref 17), the texture evolution is treated as a fluid flow in orientation space composed by Euler angles. At any point represented by g in the orientation space, the density in this orientation space is:

$$\rho = (1/8\pi^2) f(g) \sin\phi \quad \text{(Eq 9)}$$

According to the conservation principle in the orientation space, an increase in the quantity of matter in an element of volume dV should be the same as the quantity of the matter moving in dV across the surface S. The continuity equation can then be represented as

$$\oint_S f(g,\eta) \left(\frac{1}{8\pi^2}\right) \sin\phi R \cdot \hat{n} d\sigma + \frac{\partial}{\partial t} \iiint_V f(g,\eta) \left(\frac{1}{8\pi^2}\right) \sin\phi \, dV = 0 \quad \text{(Eq 10)}$$

where $R(g)$ is the flow rate. For an infinitesimal volume element in the orientation space, $dV = d\phi_1 d\phi d\phi_2$, the first term in

Eq 10 is the increase of the quantity of matter per unit time, and the second term describes the quantity of matter moving out of the infinitesimal volume element. Thus

$$\frac{\partial f(g,\eta)}{\partial t}+\frac{1}{\sin\phi}div[f(g,\eta)\sin\phi R(g)]=0 \quad \text{(Eq 11)}$$

By simplifying Eq 11, the continuity equation for the conservation of quantity of matter in a volume element in the Euler space becomes

$$\frac{\partial f(g,\eta)}{\partial t}+div[f(g,\eta)R(g)]+ctg\,\phi f(g,\eta)R(g)=0 \quad \text{(Eq 12)}$$

Using the expression for texture in Eq 6, Eq 12 is expanded in a series of spherical harmonics:

$$\sum_{lmn}\frac{dF_l^{mn}(\eta)}{d\eta}\dot{T}_l^{mn}(g)+\sum_{\lambda\sigma\rho}F_\lambda^{\sigma\rho}(\eta)\left(div\left(\dot{T}_\lambda^{\sigma\rho}(g)R(g)\right)+ctg\phi\,\dot{T}_\lambda^{\sigma\rho}(g)R(g)\right)=0 \quad \text{(Eq 13)}$$

The second summation can be further expanded into a series of generalized spherical harmonics:

$$div\left(\dot{T}_\lambda^{\sigma\rho}(g)R(g)\right)+ctg\phi\dot{T}_\lambda^{\sigma\rho}(g)R(g)=-\sum_{lmn}A_{l\lambda}^{mn\sigma\rho}\dot{T}_l^{mn}(g) \quad \text{(Eq 14)}$$

Here, $A_{l\lambda}^{mn\sigma\rho}$ is introduced as the coefficients of the spherical harmonics. By substituting Eq 14 back into Eq 13, a linear relationship between the texture coefficients and their rate of change is derived:

$$\frac{dF_l^{mn}(\eta)}{d\eta}=\sum_{\lambda\sigma\rho}A_{l\lambda}^{mn\sigma\rho}F_\lambda^{\sigma\rho}(\eta) \quad \text{(Eq 15)}$$

A similar linear relationship was used by Bunge (Ref 18-20) and Klein (Ref 23) to predict the texture evolution in the orientation space. In this study, a texture evolution function obtained by the integration of Eq 15 was used to describe the evolution of the texture coefficients with the deformation parameter:

$$F(\eta)=e^{A(\eta-\eta_0)}F(\eta_0) \quad \text{(Eq 16)}$$

Equation 16 was used to simulate the texture evolution of titanium to generate processing paths.

2.3 Texture Evolution Parameter Matrix

Texture evolution parameter matrix **A** is an intrinsic property of materials depending on a velocity gradient. Processing path function is the essence of this linear model.

The coefficients represented by the sixth rank parameter **A** can be rearranged as the elements of a matrix and will be called "texture evolution matrix" in this study. The task of this linear model, represented here by Eq 15 and 16, is to find a processing recipe to achieve the desired texture from the initial one by using our knowledge in texture evolution matrix.

In this study, Eq 16 was used to simulate the texture evolution of cold- and hot-rolled titanium at 260 °C to generate a processing path. If the number of useful texture coefficients F_l^{mn} is limited to N, then texture data at $N+1$ different strains will be needed to obtain a solution for texture evolution coefficient $A_{l\lambda}^{mn\sigma\rho}$.

It is clear that the evolution of texture is a function of the details and physics of the microstructure and the underlying deformation mechanism. All these details are embedded in the sixth-order parameter **A**, which is a function of many different other features of the microstructure such as grain size and distribution, precipitates, dislocation density, and second phase particles which can affect the evolution. All these factors will influence texture evolution during thermo-mechanical deformation, which in turn defines texture evolution matrix **A**.

2.4 Limitation of the Model

Texture is defined as "preferred orientation distribution" and is a macroscopic average representation of the orientation of crystals. A formulation based on texture does not take into account grain structure and grain boundary character as well as the grain-to-grain interaction. Texture as an ensemble average representation is only a one-point distribution function. Higher order statistics can incorporate the additional details of the microstructure (Ref 24, 25) and can be used for the evolution of the microstructure. On the other side, if the deformation mechanism is changed, the texture evolution matrix **A** will not keep constant during deformation. More tests and optimization are also needed for cases of high strain rate and high strain level.

3. Materials and Experimental

The combination of high strength-to-weight ratio, excellent mechanical properties, and corrosion resistance makes titanium suited for many critical applications. The basic commercial production process of titanium alloys, which include forgings and typical mill products, constitute more than 70% of the market in titanium alloy production. These products are the most readily available form of titanium-based materials, although cast and powder metallurgy (PM) products are also available for applications that require complex shapes or the use of PM techniques to obtain microstructures not achievable by conventional ingot metallurgy. In this study, we will concentrate on cold and hot rolling.

Another important characteristic of titanium alloys are the reversible transformation of the crystal structure from alpha (hexagonal close-packed) structure to beta (body-centered cubic) structure when the temperature exceeds certain levels. This anisotropic behavior, which depends on the type and amount of alloy contents, introduces more complex variations in microstructure and more diverse strengthening opportunities than those of other nonferrous alloys such as copper or aluminum.

There are basically four types of alloys distinguished by their microstructure: pure titanium, alpha alloys, beta alloys, and alpha-beta alloys. The material studied here is a commercial pure titanium grade 2 (Timetal 50A), provided by TIMET in the form of sheet specimens after rolling and mill annealing (ASTM-B-265). Chemical composition and mechanical properties are listed in Table 1 and 2, respectively.

The detailed description of the experimental procedure is presented elsewhere (Ref 26). The specimens were cut by Electric Discharge Machining (EDM) equipment. The size of working samples used on the thermo-mechanical processing is 2.5 cm × 7.6 cm × 1.6 cm. The cutting surfaces, which also are

Table 1 Chemical composition (wt.%) of commercial pure titanium

Material	O	C	N	Fe	H	Residual elements	Titanium
Commercial pure Ti	0.25	0.008	0.03	0.30	0.015	0.40	Remainder

Table 2 Mechanical properties of commercial pure titanium at room temperature and 300 °C

Temperature, °C	Yield strength, MPa	UTS, MPa	Elongation, %
25	345	485	28
300	127	229	43

the rolling planes in this study, were ground and polished to remove the thermally affected layer to reduce the possibility of external influence from the previous machining of the as-received material.

The thermo-mechanical processing of the samples was conducted by a conventional two-high rolling mill. Samples of the as-received titanium sheets were processed in two categories: cold rolled at room temperature (25 °C) and hot rolled at 260 °C. Same degrees of reduction were chosen at both rolling temperatures: 20%, 40%, 60%, 80%, and 95%. In order to obtain a homogeneous deformation, a step size of 5% reduction was applied. Before and after each pass of 5%, the sample was homogenized at the required temperature for 30 min. The procedure was repeated until the desired reduction level was achieved. After the final step, the samples were cooled in air.

The texture measurements were performed using a Philips X'Pert PW 3040 MRD equipped with texture goniometer. Voltage and current was set up at 40 kV and 45 mA. Five incomplete pole figures, (0002), (1011), (1012), (1120), and (1013), were scanned in a 5° by 5° grid for tilt angle and radiation angle, using Cu Kα radiation, point source, 1 mm × 1 mm cross slit and 1 mm receiving slit. PopLA software package (Ref 27) was used to generate orientation distribution function (ODF). Textures coefficients calculated from ODF will be used in our processing path model.

4. Results and Discussions

The as-received sample has a weak texture. (0001) pole figure of the undeformed sample is illustrated in Fig. 1. The sample coordinate according to the convention adopted here composed of rolling direction (RD), transverse direction (TD), and normal direction (ND). The sample is very isotropic after annealing. Maximum intensity in (0001) pole figure is only two times random.

For each of the thermo-mechanical processes conducted, texture was characterized at strains of 20%, 40%, 60%, 80%, and 95%, respectively. In this study, only results from strains of 20% and 80% are shown to avoid redundancy.

From our previous studies (Ref 7, 8), we concluded that five data points are not enough to feed into the processing path model to initiate a reliable simulation. In order to solve this problem, a linear interpolation has been performed between

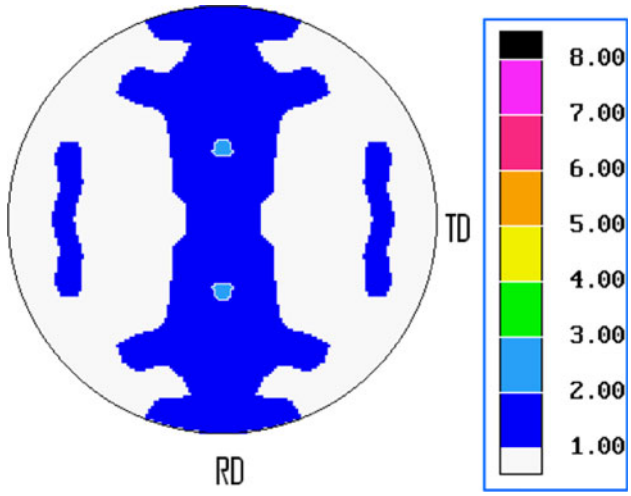

Fig. 1 (0001) pole figure of non-deformed titanium sample

Table 3 Increase of size of the texture evolution matrix A with truncation order ℓ_{max}

ℓ_{max}	4	8	12	18	22
Size of **A**	6*6	27*27	69*69	202*202	351*351

each point to generate necessary large numbers of data points from 0% to 100%. In the previous study, we also observed that a step size of 0.2% gave us the best results; therefore, for this study, we continue to use a step size of 0.2%.

In Sect 4.1, the streamlines of thermo-mechanical deformations are visualized in material hull. Next, in Sect 4.2, texture evolution matrix was calculated from the processing path model. The simulated results were verified by the mean root square error created by the truncation of the expansion in the Fourier series. Like in our previous studies (Ref 7, 8), spherical harmonics expansion was truncated at order ℓ_{max} of 4, 8, 12, 18, and 22, respectively.

How to simulate the processing path precisely and efficiently is a critical question in the processing path model. It depends on the calibration of texture evolution matrix **A**. When the definition of texture is truncated at higher order ℓ_{max}, the size of matrix **A** will be larger, the computation time will be longer, and the simulation error will be smaller (Ref 7, 8). Table 3 lists the relationship between the truncation order ℓ_{max} and the size of the matrix **A**.

Section 4.3 visualizes the error using the pole figures at different thermo-mechanical deformation first, then the regression curves.

Since the crystal system is hexagonal compact (hcp), when $\ell_{max} = 4$, Eq 6 becomes

$$\begin{aligned} f(g) &= \sum_{l=0}^{L_{max}} \sum_{m=0}^{M(l)} \sum_{n=0}^{N(l)} F_l^{mn} \dot{T}_l^{mn}(g) \\ &= F_0^{11} \dot{T}_0^{11}(g) + F_2^{11} \dot{T}_2^{11}(g) + F_2^{12} \dot{T}_2^{12}(g) + F_4^{11} \dot{T}_4^{11}(g) \\ &\quad + F_4^{12} \dot{T}_4^{12}(g) + F_4^{13} \dot{T}_4^{13}(g) = \dot{T}_0^{11}(g) + F_2^{11} \dot{T}_0^{11}(g) \\ &\quad + F_2^{12} \dot{T}_2^{12}(g) + F_4^{11} \dot{T}_4^{11}(g) + F_4^{12} \dot{T}_4^{12}(g) + F_4^{13} \dot{T}_4^{13}(g) \end{aligned} \quad \text{(Eq 17)}$$

For each truncation order ℓ_{max}, the size of the texture evolution matrix is presented in Table 3.

4.1 Texture Evolution in Materials Hull

Texture coefficients F_l^{mn} were obtained from the experimental measurement of pole figures. The more texture coefficients are used in the representation, the more precise the texture is described. In correlating the texture and elastic properties, 5 texture coefficients are needed for hcp materials, which are F_2^{11}, F_2^{12}, F_4^{11}, F_4^{12}, and F_4^{13}. Their evolution during warm and cold rolling is illustrated in Fig. 2.

One can easily notice a trend in the evolution of the texture coefficients; it seems that F_2^{11} and F_4^{11} follow the same path. In the cold-rolled case, their value increases in a wave-like shape in function of the deformation strain. In the case of hot rolled, their value increases up to a strain of 80% and then drops. F_2^{12} and F_4^{12} follow a similar path, with their values diminishing with the increase in strain. F_4^{13} follows its own path while staying close to 0.

In MSD, texture in materials is represented by a set of texture coefficients. In a space composed of the texture coefficients, each point corresponds to a specific texture. All of the possible textures are in a subspace confined by microstructure hull. In order to visualize the processing path in the materials hull, two 3D subspaces are used in Fig. 3. One is composed of F_2^{11}, F_2^{12}, and F_4^{11} (Fig. 3a). Another one is composed of F_4^{11}, F_4^{12}, and F_4^{13} (Fig. 3b). The processing paths, represented by the big squares, demonstrate the evolution of texture coefficients during cold and hot rolling to a strain of 0.95. The wired frame, the microstructure hull, illustrates the limiting values of texture coefficients. All possible microstructures are confined in the microstructure hull. No microstructure exists outside the hull. It is clear that the microstructures involved in hot rolling of commercially pure titanium (strained up to 0.95) only occupy a small subset in the microstructure space. Each microstructure in the space has its own corresponding property. The relatively small processing path in the microstructure space illustrates how limited the properties have been utilized in titanium.

4.2 Effects of the Increase of ℓ_{max} on the Prediction of F_2^{11}, F_2^{12}, F_4^{11}, F_4^{12}, and F_4^{13}

In this section, we studied the influence of ℓ_{max} on the evolution of individual texture coefficients such as F_2^{11}, F_2^{12}, F_4^{11}, F_4^{12}, and F_4^{13}. After texture evolution was simulated from processing path model, the truncation error,

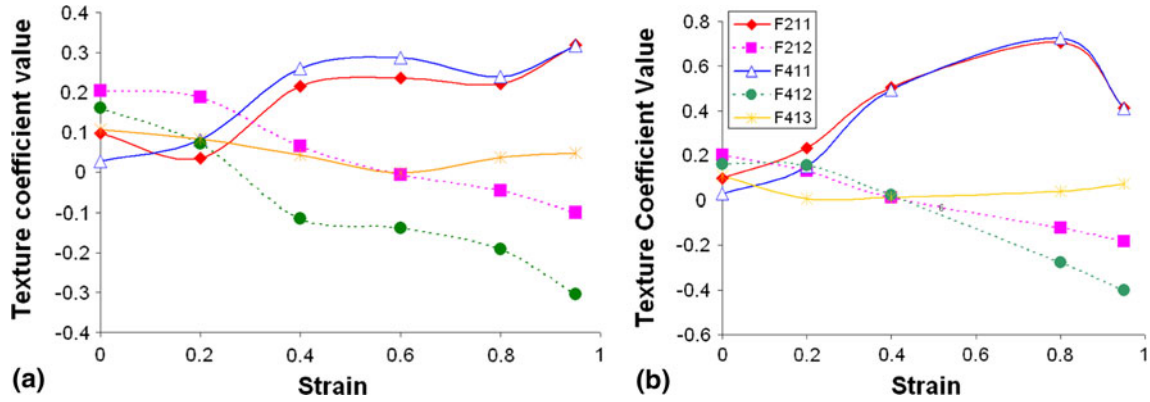

Fig. 2 Evolution of the texture coefficients, F_2^{11}, F_2^{12}, F_4^{11}, F_4^{12}, and F_4^{13}, during rolling in titanium: (a) at room temperature, (b) at 260 °C

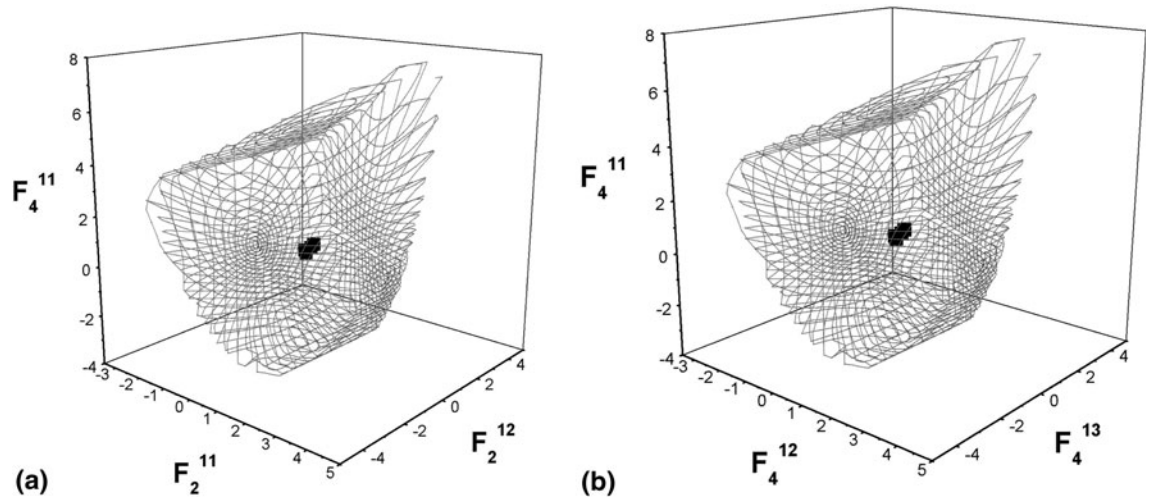

Fig. 3 Processing path of titanium during rolling to a strain of 0.95 in microstructure hull (a) in a material subspace composed of (F_4^{11}, F_2^{11}, F_2^{12}), (b) in a material subspace composed of (F_4^{11}, F_4^{12}, F_4^{13})

error_l^{mn}, between the simulated results and experimental data was calculated according to Eq 18:

$$\text{error}_l^{mn} = \frac{1}{N}\sqrt{\sum_{i=1}^{N}\left({}^{i}F_{l\ \text{recalculated}}^{mn} - {}^{i}F_{l\ \text{experimental}}^{mn}\right)^2} \qquad \text{(Eq 18)}$$

N is the number of data points chosen in the range of deformation strain chosen. In this case, six points are chosen, at rolling strains of 0, 0.2, 0.4, 0.6, 0.8, and 1.0, respectively.

Figures 4 and 5, represent, respectively, the error evolution for the cold and hot rolled specimens at 260 °C of the F_2^{11}, F_2^{12}, F_4^{11}, F_4^{12}, and F_4^{13} texture coefficients.

In the case of room temperature, the higher errors are in the order of 10^{-2}; whereas for the hot-rolled specimens, the root mean square difference is ten times higher. For all cases, it is clear that the curves follow the same pattern: as $\ell_{\max}$ increases, the errors diminish and are almost null for $\ell_{\max} = 22$.

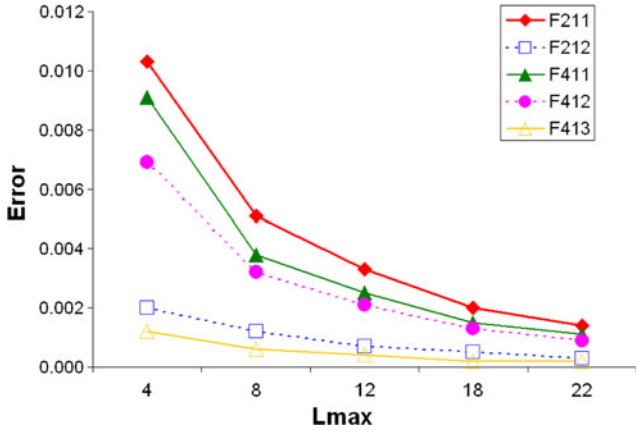

Fig. 4 Error evolution for cold rolled of the F_2^{11}, F_2^{12}, F_4^{11}, F_4^{12}, and F_4^{13} texture coefficients

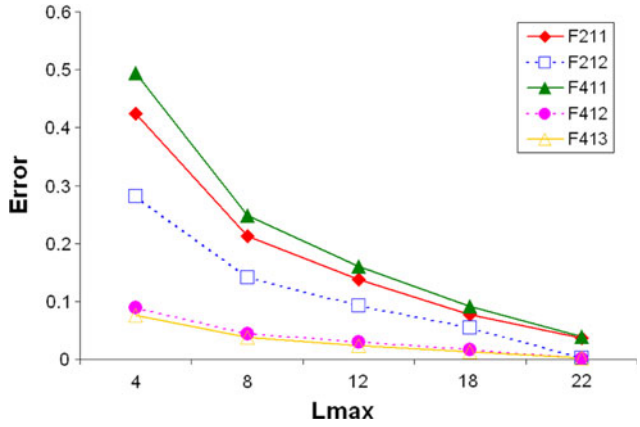

Fig. 5 Error evolution for hot rolled at 260 °C of the F_2^{11}, F_2^{12}, F_4^{11}, F_4^{12}, and F_4^{13} texture coefficients

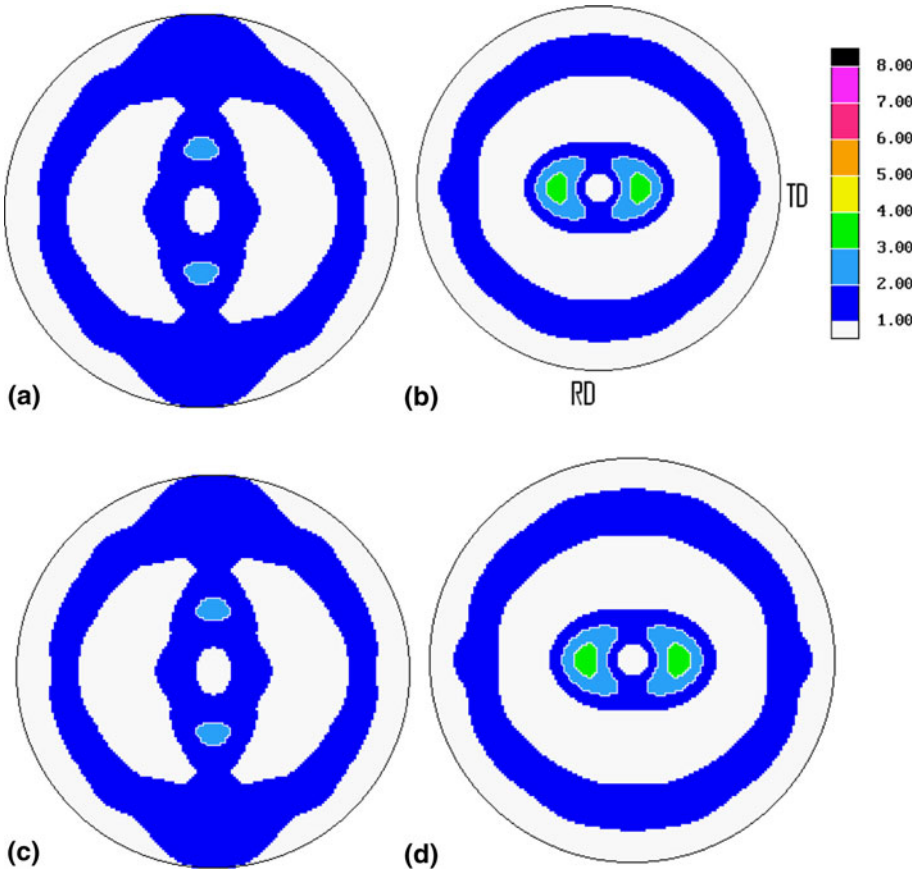

Fig. 6 Experimental and simulated (0001) pole figures of titanium during cold rolling at different strain. (a) Experimental pole figures at a strain of 20%. (b) Experimental at a strain of 80%. (c) Simulated at a strain of 20%. (d) Simulated at a strain of 80%

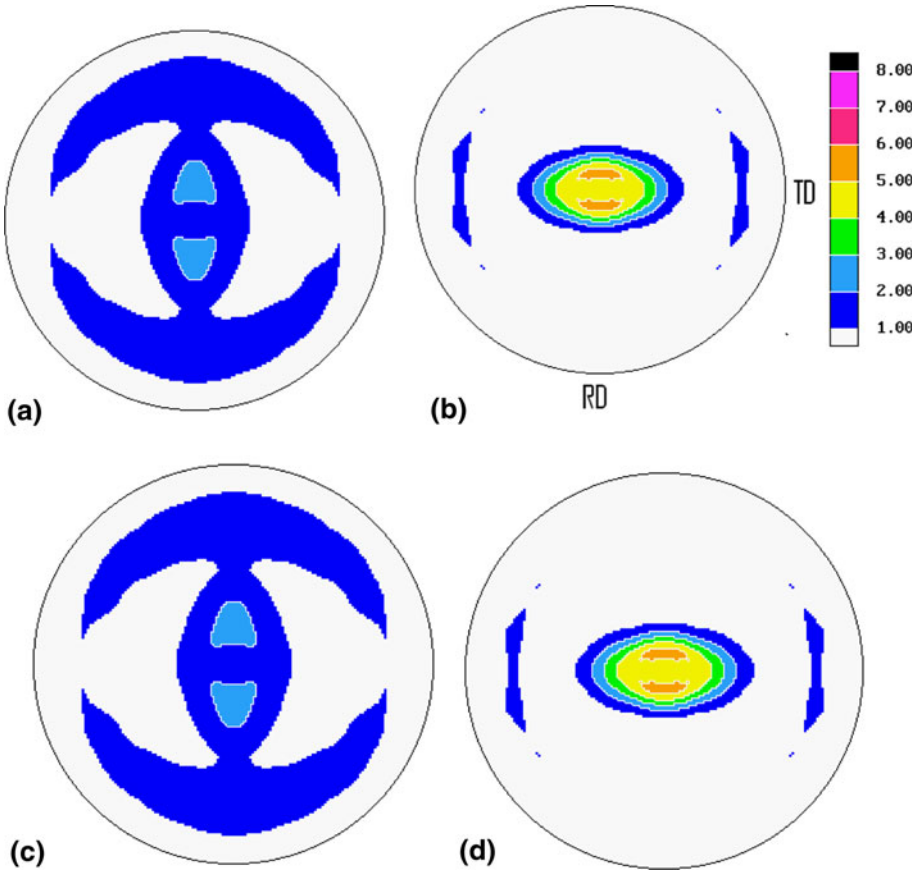

Fig. 7 Experimental and simulated (0001) pole figures of titanium during hot rolled rolling at different strain. (a) Experimental pole figures at a strain of 20%. (b) Experimental pole figure at a strain of 80%. (c) Simulated pole figure at a strain of 20%. (d) Simulated pole figure at a strain of 80%

Accordingly, we can conclude that the processing path model is able to predict precisely the texture after thermo-mechanical deformation when order in the texture evolution matrix $\ell_{max} = 22$.

4.3 Comparison of Simulated Texture and Experimental Results

After hot rolling at different strains, the experimental data obtained by x-ray diffraction were used to recalculate the (0001) pole figures. These pole figures are shown in Fig. 6(a) and (b) for room temperature and Fig. 7(a) and (b) for the hot-rolled samples. When the sample is rolled to a strain of 20%, (0001) axes of crystals starts to concentrate on the plane of TD (transverse direction) and ND (normal direction). With the increase of rolling strain, this texture component rotates closer to ND. The split from ND becomes smaller. The simulated results are shown in Fig. 6(c) and (d) for room temperature and Fig. 7(c) and (d) for the hot rolled samples. Figures 6 and 7 clearly demonstrate that processing path model is able to accurately predict the evolution of the pole figures. After the texture evolution matrix **A** is calculated from the experimental results, using this **A** will predict texture evolution of the same materials deformed by the same mechanism.

5. Conclusion

Processing path model, based on a conservation principle in the orientation space, linearly describes texture evolution during thermomechanical deformation by texture evolution matrix. It provides a common language between process and microstructure. This study described in detail how to use processing path model to simulate texture evolution during thermomechanical deformation for polycrystalline metals. We used this model to predict texture evolution of commercial pure alpha titanium after cold rolling and hot rolling respectively. Root mean square errors were computed from the experimental texture coefficients and predicted results. The simulated results agree well with experimental data. By visualizing texture evolution as processing paths within the microstructure hull, it is found that hot and cold rolling of titanium can only reach a very limited range of the possible microstructures that titanium polycrystalline materials may reach. It would be interesting to pursue this further and study more methods of deformation and processing that would produce pure titanium with new microstructure and properties.

Acknowledgments

This study has been funded under the AFOSR grant # F49620-03-1-0011. The authors acknowledge the grant form Pacific Northwest National Lab# 1806C44.

References

1. E.W. Collings, *The Physical Metallurgy of Titanium Alloys*, ASM, Metals Park, OH, 1994

2. B.L. Adams, A. Henrie, B. Henrie, M. Lyon, S.R. Kalidindi, and H. Garmestani, Microstructure-Sensitive Design of a Compliant Beam, *J. Mech. Phys. Solids*, 2001, **49**, p 1639–1663
3. B.L. Adams, M. Lyon, and B. Henrie, Microstructure by Design: Linear Problems in Elastic-Plastic Design, *Int. J. Plast.*, 2004, **20**, p 1577–1602
4. D.S. Li, H. Garmestani, and B.L. Adams, A Processing Path Model for Texture Evolution in Cubic-Orthotropic Polycrystalline System, *Int. J. Plast.*, 2005, **21**(8), p 1591–1617
5. D.S. Li, H. Garmestani, and S. Ahzi, Processing Path Optimization to Achieve Desired Texture for Polycrystalline Materials, *Acta Mater.*, 2007, **55**(2), p 647–654
6. D.S. Li, H. Garmestani, and S.E. Schoenfeld, Evolution of Crystal Orientation Distribution Coefficients During Plastic Deformation, *Scr. Mater.*, 2003, **49**, p 867–872
7. D.S. Li, J. Bouhattate, and H. Garmestani, Processing path Model to Describe Texture Evolution During Mechanical Processing, *Mater. Sci. Forum*, 2005, **495–497**, p 977–982
8. J. Bouhattate, D.S. Li, H. Garmestani, S. Ahzi, and M. Khaleel, On Improving Predictions of Texture Evolution Using Processing Path Model, *Mat.-wiss. u. Werkstofftech.*, 2005, **36**(10), p 538–540
9. M. Lyon and B.L. Adams, Gradient-Based Non-Linear Microstructure Design, *J. Mech. Phys. Solids*, 2004, **52**, p 2569–2586
10. G. Proust and S.R. Kalidindi, Procedures for Construction of Anisotropic Elastic-Plastic Property Closures for Face-Centered Cubic Polycrystals Using First Order Bounding Relations, *J. Mech. Phys. Solids*, 2006, **54**(8), p 1744–1762
11. X.P. Wu, S.R. Kalidindi, and C. Necker, Modeling Anisotropic Stress-Strain Response and Crystallographic Texture Evolution in alpha-Titanium during Large Plastic Deformation using Taylor-Type Models: Influence of Initial Texture and Purity, *Metall. Mater. Trans.*, 2008, **A39**, p 3046–3054
12. Y. Wang, N. Ma, Q. Chen, F. Zhang, S.L. Chen, and Y.A. Chang, Predicting Phase Equilibrium, Phase Transformation, and Microstructure Evolution in Titanium Alloys, *JOM*, 2005, **57**, p 32–39
13. Y.B. Chun, S.L. Semiatin, and S.K. Hwang, Monte Carlo Modeling of Microstructure Evolution During the Static Recrystallization of Cold-Rolled, Commercial-Purity Titanium, *Acta Mater.*, 2006, **54**, p 3673–3689
14. S. Balasubramanian and L. Anand, Plasticity of Initially Textured Hexagonal Polycrystals at High Homologous Temperatures: Application to Titanium, *Acta Mater.*, 2002, **50**, p 133–148
15. D.M. Park and S. Ahzi, Polycrystalline Plastic Deformation and Texture Evolution for Crystals Lacking Five Independent Slip Systems, *J. Mech. Phys. Solids*, 1990, **38**, p 701–724
16. A. Clement and P. Coulomb, Eulerian Simulation of Deformation Textures, *Scr. Metall.*, 1979, **13**, p 899–901
17. A. Clement, Prediction of Deformation Texture Using a Physical Principle of Conservation, *Mater. Sci. Eng.*, 1982, **55**, p 203–210
18. H.J. Bunge and C. Esling, Texture Development by Plastic Deformation, *Scr. Metall.*, 1984, **18**, p 191–195
19. H.J. Bunge, *Texture Analysis in Materials Science: Mathematical Methods*, Butterworth & Co, London, 1982
20. H.J. Bunge, R. Kiewel, Th. Reinert, and L. Fritsche, Elastic Properties of Polycrystals—Influence of Texture and Stereology, *J. Mech. Phys. Solids*, 2000, **48**, p 29–66
21. H. Garmestani, P. Kalu, and D. Dingley, Micro-Characterization of Al-8090 Superplastic Materials Using Orientation Imaging Microscopy, *J. Mater. Sci. Eng. A.*, 1998, **242/1-2**, p 284–291
22. H. Garmestani and K. Harris, Orientation Determination by EBSP in an Environmental Scanning Electron Microscope, *Scr. Metall.*, 1999, **41**(1), p 47–53
23. H. Klein and H.J. Bunge, Modeling Deformation Texture Formation by Orientation Flow-Fields, *Steel Res.*, 1991, **62**, p 548–559
24. G. Jefferson, H. Garmestani, R. Tannenbaum, and E. Todd, Two-point Probability Distribution Functions: Application to Block Co-Polymer Nanocomposites, *Int. J. Plast.*, 2005, **21**, p 185–198
25. G. Saheli, H. Garmestani, and B.L. Adams, Microstructure Design of a Two Phase Composite Using Two-Point Correlation Functions, *J. Comput. Aid. Mater. Des.*, 2004, **11**, p 103–115
26. I.C. Dragomir, D.S. Li, G.A. Castello-Branco, H. Garmestani, R.L. Snyder, G. Ribarik, and T. Ungar, Evolution of Dislocation Density and Character in Hot Rolled Titanium Determined by X-Ray Diffraction, *J. Mater. Character.*, 2005, **55**, p 66–74
27. J.S. Kallend, U.F. Kocks, A.D. Rollett, and H.R. Wenk, Operational Texture Analysis, *Mater. Sci. Eng.*, 1991, **A132**, p 1–11